PHYSICAL REVIEW B **81**, 161101(R) (2010)

Metallicity in $LaTiO_3$ thin films induced by lattice deformation

Franklin J. Wong,[1,2] Seung-Hyub Baek,[3] Rajesh V. Chopdekar,[1] Virat V. Mehta,[1,2] Ho-Won Jang,[3] Chang-Beom Eom,[3] and Yuri Suzuki[1,2]

[1]*Department of Materials Science and Engineering, University of California, Berkeley, California 94720, USA*

[2]*Materials Sciences Division, Lawrence Berkeley National Laboratory, Berkeley, California 94720, USA*

[3]*Department of Materials Science and Engineering, University of Wisconsin, Madison, Wisconsin 53706, USA*

(Received 2 October 2009; revised manuscript received 8 December 2009; published 15 April 2010)

Orthorhombic bulk $LaTiO_3$ is a correlated Mott insulator whose delicate antiferromagnetic insulating ground state can be easily destroyed by cation vacancies, excess oxygen, or alkaline-earth dopants, resulting in metallicity. Here we show that metallic conduction can also be realized in epitaxial $LaTiO_3$ thin films on (001) $SrTiO_3$ substrates, while films grown on (110) $DyScO_3$ and $GdScO_3$ substrates are insulating. These results illustrate the sensitivity of electrical transport to lattice effects and demonstrate the tunability of correlated oxide thin-film properties via substrate-induced deformation.

DOI: 10.1103/PhysRevB.81.161101 PACS number(s): 71.30.+h, 81.15.−z, 73.61.−r, 72.80.Ga

Metal-insulator transitions have been extensively studied in an effort to understand the mechanism(s) underlying the localization of carriers in a wide range of correlated materials. Electron correlation plays a critical role in complex oxides, including colossal magnetoresistive materials and high-T_C superconductors. The Mott insulator $LaTiO_3$ has received renewed interest in light of the recent discovery of metallicity in (001) perovskite $LaTiO_3/SrTiO_3$ superlattices.[1,2] At the $LaTiO_3/SrTiO_3$ Mott insulator/band insulator heterointerface, localized electrons from the correlated Mott insulator are thought to be transferred into the band insulator, creating a confined channel where the carriers can become mobile.[1–8]

In addition to charge transfer at the interface, lattice distortions need to be taken into consideration in such oxide heterostructures. More recently, a dynamical mean-field model of $LaTiO_3/SrTiO_3$ superlattices predicts metallicity in tetragonally strained $LaTiO_3$ due to a change in sign and decrease in magnitude of the crystal-field splitting of t_{2g} bands compared to bulk orthorhombic $LaTiO_3$.[9] While this model assumes ideal tetragonal distortions without any tilting or rotation of the oxygen octahedra, it illustrates the sensitivity of $LaTiO_3$ to structural distortions as well as highlights the prospects in manipulating electronic properties of related materials through lattice deformation.

In this Rapid Communication, we show that lattice distortions in $LaTiO_{3+\delta}$ (LTO) thin films that are coherently grown on lattice-mismatched $SrTiO_3$ (STO) substrates give rise to metallic conductance that scales with film thickness. In contrast, LTO films grown under identical growth conditions but under smaller in-plane (IP) compressive epitaxial strain on $DyScO_3$ (DSO) and $GdScO_3$ (GSO) substrates are insulating. From our studies, we conclude that the effects of lattice deformation must be carefully considered in conjunction with interfacial phenomena in order to explain the recent novel electrical transport behavior found in LTO/STO heterostructures.

Bulk $LaTiO_3$ is a Mott insulator that has a $GdFeO_3$ orthorhombic structure.[10] It is on the verge of a metal-insulator transition with a small optical band gap of ~0.1 eV.[11] The effects of chemical doping[12–18] and hydrostatic pressure[12] have been investigated extensively in bulk LTO in order to study the roles of electronic bandwidth and band filling. Metallicity in LTO can be induced by cation vacancies, excess oxygen, or alkaline-earth doping of the rare-earth site.[12–18] There have been thin-film studies of LTO (Refs. 19–21) and Sr-doped LTO,[22] but the effects of structural distortions due to epitaxial strain on the transport properties have not been examined experimentally.

LTO films were deposited by pulsed-laser deposition from a powder-pressed $La_2Ti_2O_7$ target onto cubic (001) STO substrates with a lattice parameter of 3.905 Å as well as orthorhombic (110) $GdScO_3$ and $DyScO_3$ substrates, with pseudocubic lattice parameters of 3.968 and 3.942 Å, respectively. The bulk average pseudocubic lattice parameter of LTO is ~3.97 Å.[16] In this Rapid Communication, we will use pseudocubic indices for plane and direction notation. The films were grown in vacuum of $\sim 5 \times 10^{-6}$ Torr, at 625 °C, with a 248 nm KrF excimer laser operating at 3 Hz, and ~1.4 J/cm^2 laser fluence. Ohtomo *et al.* found that pulsed-laser deposition can stabilize the more reduced stoichiometric $LaTiO_3$ phase starting from an oxygen-rich $La_2Ti_2O_7$ target, the more readily achievable bulk stoichiometry.[19] Rutherford backscattering spectroscopy (RBS) verified the 1:1 stoichiometric ratio of La to Ti cations, to within the error of measurement, and also determined that the thickness of the different films range from 15 to 45 nm. Atomic force microscopy images of the LTO films on all three substrates showed atomically smooth surfaces.

Figure 1(a) is a high-resolution cross-sectional transmission electron microscopy (TEM) image of a LTO film on a STO substrate (LTO/STO) at the film/substrate interface, showing epitaxial film growth. Epitaxial growth is further confirmed by the Fourier transform of the image, indicating that the film is single phase and isostructural to the substrate. Upon taking numerous images at different locations and magnifications on the sample, we have not observed any indication of the oxygen-rich $La_2Ti_2O_7$ phase, whose structure in bulk[23] and thin-film[19,24] form have been reported in previous TEM studies. Therefore, we expect our samples to be nearly stoichiometric $LaTiO_3$.

X-ray diffraction indicated the tetragonal distortions in the LTO/STO films. θ-2θ scans revealed only 00l film reflections. Reciprocal space maps (RSMs) of the 103 LTO peak

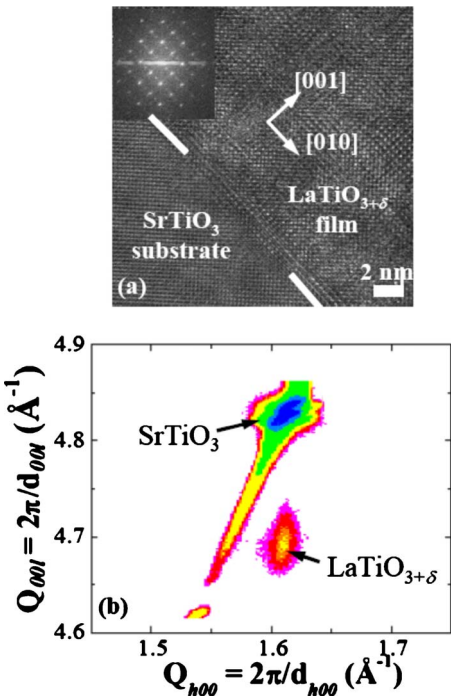

FIG. 1. (Color online) (a) A representative cross-sectional TEM image along the [100] zone axis of a LTO/STO film. The inset is the fast Fourier transform of the image. (b) RSM of the 103 reflection of the 34 nm LTO/STO sample.

enabled us to deduce both IP and out-of-plane (OOP) lattice parameters of the LTO films. Figure 1(b) is a RSM of the 103 reflection peak of a 34 nm LTO/STO with IP and OOP lattice parameters of 3.905 and 4.015 Å, respectively. The intensity streak corresponding to the substrate peak is caused by the line-focused shape of the x-ray beam. The 103 reflection peaks of 34 nm films on DSO and GSO substrates were likewise mapped out to determine IP and OOP lattice parameters (Table I). The small degree of orthorhombic IP distortion from the scandate substrates amounts to less than 0.005 Å difference in IP interplanar spacings, which is difficult to detect in the thin films. All of the films are coherently strained IP to conform to the underlying substrates. However, it must be noted that bond lengths and bond angles are not explicitly measured and are difficult to determine in such thin films. The small full-width-at-half-maximum values (<0.1°) of the 002 reflection rocking curves confirm high thin-film crystalline quality.

Electrical transport measurements in the van der Pauw

TABLE I. (Color online) IP and OOP parameters (a and c) of 34 nm LTO films grown on different substrates. Volume dilation and tetragonal distortions are decoupled.

Substrate	a (Å)	c (Å)	FWHM (deg)[a]	$\varepsilon_{xx}+\varepsilon_{yy}+\varepsilon_{zz}$ (%)	$2\varepsilon_{zz}-\varepsilon_{xx}-\varepsilon_{yy}$ (%)
$GdScO_3$	3.968	3.991	0.075	0.43	1.16
$DyScO_3$	3.944	4.014	0.07	−0.20	3.52
$SrTiO_3$	3.905	4.015	0.06	−2.14	5.54

[a]Of the 002 diffraction peak.

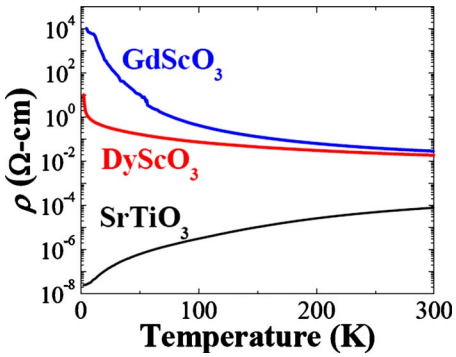

FIG. 2. (Color online) Resistivity curves of the three 34 nm LTO/STO, LTO/DSO, and LTO/GSO samples. Difficulties in maintaining an Ohmic contact on an insulating sample contributed to the low-temperature noise observed in LTO/GSO.

geometry were performed on the films. Figure 2 shows resistivity curves of 34 nm LTO/STO and LTO films of the same thickness grown on DSO and GSO (LTO/DSO and LTO/GSO, respectively) under the same deposition conditions. While LTO/STO displays metallic behavior, both LTO/DSO and LTO/GSO are insulating—although LTO/GSO exhibits higher resistivity than LTO/DSO over the entire measured temperature range.

Furthermore, LTO/STO films are metallic for all film thicknesses. Figure 3(a) shows that the resistivity curves of the different samples overlay one another. The relatively high magnitude and temperature dependence of the resistivity values are comparable to those of the metallic d^1 perovskite oxide ReO_3.[25] The inverse scaling of sheet resistance with film thickness at 300 K can be seen in Fig. 3(b). In Fig. 3(c), we see specifically that the sheet carrier concentration values increase roughly linearly with film thickness. This scaling is evidence that metallic conduction occurs in the entire film.

We also performed Hall-effect measurements on the 34 nm LTO/STO film to decouple the carrier concentration and mobility (Fig. 4). The carriers are electronlike. The carrier concentration is fairly temperature independent and corresponds to an average of 0.77 electrons per Ti ion. Its Hall

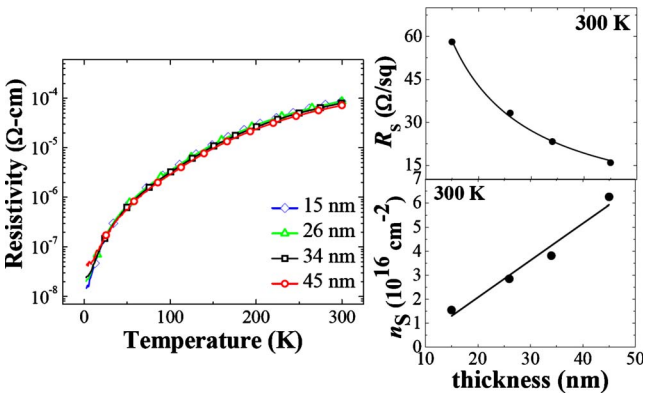

FIG. 3. (Color online) (a) Resistivity of LTO/STO films of different thicknesses. Film thickness-dependent variations in (b) sheet resistance and the (c) sheet carrier concentration measured at 300 K. The fitted lines show inverse and proportional thickness dependence, respectively.

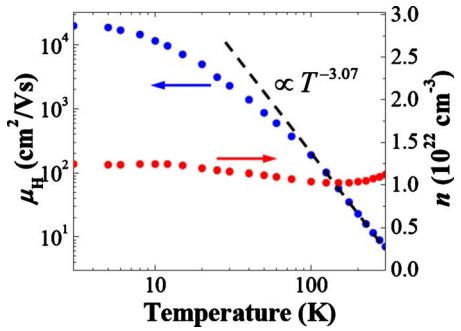

FIG. 4. (Color online) Hall mobility (μ_H) and carrier concentration (n) of 34 nm LTO/STO.

mobility has a power-law dependence at high temperatures, $\mu_H \propto T^{-3.07}$, likely to be dominated by carrier interaction with optical phonons. At low temperatures, the resistivity is governed by scattering by defects in and at the boundaries of the sample, and the mobility saturates to $\sim 10^4$ cm^2/Vs.

Given the insulating LTO/DSO and LTO/GSO samples, metallicity in LTO/STO cannot be explained by the formation of off-stoichiometric point defects in the LTO solely relating to thin-film growth. However, unintentional Sr doping of LTO or La doping of STO, oxygen vacancies in the STO substrate, and electronic reconstruction at the LTO/STO heterointerface are other possible origins of metallicity.

Our results cannot be accounted for by any one or combination of such sources. RBS analysis indicated that interdiffusion was negligible compared to the film thicknesses and could not have produced the large carrier densities observed in the LTO/STO samples. We have also grown a 17 nm LTO film on a STO substrate with a thin $EuTiO_3$ (ETO) buffer layer, providing a diffusion barrier to Sr from the substrate to the film and La from the film to the substrate. The resistivity curve of LTO (17 nm)/ETO (10 nm)/STO almost perfectly overlays that of a 17 nm film grown directly on a STO substrate (both not shown). This result indicates that La/Sr interdiffusion at the film/substrate interface cannot explain the metallicity. Another possible source of metallicity is oxygen vacancies in STO substrates. First, given the deposition times and oxygen (vacancy) diffusion constants,[26] the carrier concentration numbers cannot be explained in terms of reduced STO substrates. In addition, to explicitly eliminate this possibility as the origin of our metallic LTO/STO samples, we have annealed a bare STO substrate and deposited a single 10 nm ETO film on a STO substrate in growth conditions identical to those of LTO and found that these two samples were too insulating to be measured electrically. Furthermore, the nearly proportional scaling of sheet conductance and sheet carrier concentration with film thickness as shown in Fig. 3 indicates that the conductivity arises from the film itself. We also synthesized a 15 nm LTO film on a DSO substrate with a 10 nm STO buffer layer as well as just a 10 nm STO film on DSO. Neither the LTO film nor buffer layer alone exhibited metallicity, thus indicating that neither defects in the STO nor interdiffusion at the LTO/STO interface is the origin of the metallicity.

The metallic behavior of LTO/STO versus the insulating behavior of LTO/DSO and LTO/GSO can be correlated with the structure of the LTO films. Since detailed structural characterization indicates that the LTO films are coherently grown on all substrates with a high degree of crystallinity and smooth surfaces, the electronic transition cannot be attributed to differences in microstructure or defect structure.

Our findings indicate that lattice distortions profoundly modify the electronic structure of LTO. Ishida and Liebsch considered ideal tetragonal distortions in $LaTiO_3$ and found broadening of the t_{2g} bands compared to the orthorhombic bulk.[9] Their calculations show that tetragonally distorted $LaTiO_3$ on STO exhibits metallicity, whereas orthorhombic bulk $LaTiO_3$ is an insulator. The metallicity we observe in LTO/STO samples is qualitatively consistent with their claim that suppression of bulk $GdFeO_3$-type orthorhombic distortion, reduced magnitude of t_{2g} band splitting, and enhanced electron bandwidth near the Fermi level are important factors in stabilizing a metallic ground state in tetragonally deformed LTO.

From the IP and OOP lattice parameters measured, we can deduce the volume dilation $\epsilon_{xx}+\epsilon_{yy}+\epsilon_{zz}$ and an element representing the degree of volume-preserving tetragonal distortion $2\epsilon_{zz}-\epsilon_{xx}-\epsilon_{yy}$ (Table I). In LTO/GSO, the film is virtually lattice-matched with the substrate; hence, there is little IP compression. In LTO/DSO, the film is under a slight compressive strain (−0.7%) and exhibits resistivity values from a factor of about two at room temperature to more than two orders of magnitude at low temperatures lower than those of LTO/GSO. Finally, under a larger compressive strain (−1.6%), LTO/STO films undergo a lattice-induced insulator-metal transition. This trend suggests that suppressing the bulk orthorhombic structure in LTO/STO is key in inducing metallicity. It appears that on STO, the strained LTO film is distorted to the degree that its kinetic energy—electronic bandwidth—overwhelms the potential energy—on-site repulsion energy. Although the distortions in LTO/DSO are insufficient to induce metallicity, we speculate lattice effects produce a larger bandwidth of occupied states and hence higher conductance of LTO/DSO compared to those of LTO/GSO.

Given the high mobility values measured in LTO/STO samples, we speculate that electron-electron interactions intrinsic to $LaTiO_3$ are not strong enough to limit the mobility of the LTO/STO films. In addition, the role of screening effects at the LTO film/substrate interface must also be considered since STO has a high and highly temperature-dependent dielectric constant, whereas the dielectric constants of DSO and GSO are lower and vary much less with temperature. The fact that we do not observe metallic behavior in the LTO film on a 10 nm STO-buffered DSO substrate suggests that dielectric screening is not the primary cause of metallicity, but may have a second-order effect on carrier itinerancy, possibly inducing the observed high mobility; dielectric screening from the substrate on the thin film is an important topic that warrants further investigation in our and related materials systems. While we cannot completely decouple the effects of screening at the interface, the transport properties over a range of film thicknesses in LTO/STO indicate that lattice distortions play a dominant role in inducing metallicity in LTO thin films.

In conclusion, we have demonstrated how lattice distor-

tions in LTO/STO films can generate metallicity that has not been observed in the orthorhombic bulk. Though interfacial electronic reconstruction effects may also be present in our LTO/STO samples, we have shown strong evidence that metallic conduction is exhibited in the entire LTO film, and not just from a confined interface or defective STO substrate. Ultimately, understanding the electronic effects of lattice deformation may enable us to exploit substrate-induced lattice distortions to engineer systematically properties in perovskite oxide heterostructures inaccessible in bulk materials of the same stoichiometry.

The authors gratefully acknowledge financial support at Berkeley from the Director, Office of Science, Office of Basic Energy Sciences, Division of Materials Sciences and Engineering, of the U.S. Department of Energy under Contract No. DE-AC02–05CH11231. The RSM measurements performed at Madison were supported by the National Science Foundation Contract No. ECCS-0708759, the Packard Foundation, and the Office of Naval Research Contract No. N00014–07–1-0215. RVC was supported by NSF Contract No. DMR0604277. The authors would like to thank K. M. Yu for his assistance in Rutherford backscattering measurements. F.J.W. and Y.S. would like to thank T. H. Geballe and N. A. Spaldin for thoughtful discussions. The electron microscopy work was performed on the Philips 300 kV FEG in the National Center for Electron Microscopy, Lawrence Berkeley National Laboratory. F.J.W. would like to acknowledge C. Song for technical assistance and microscopy training.

[1] A. Ohtomo, D. A. Muller, J. L. Grazul, and H. Y. Hwang, Nature (London) **419**, 378 (2002).
[2] K. Shibuya, T. Ohnishi, M. Kawasaki, H. Koinuma, and M. Lippmaa, Jpn. J. Appl. Phys. **43**, L1178 (2004).
[3] S. Okamoto and A. J. Millis, Phys. Rev. B **70**, 075101 (2004).
[4] Z. S. Popovic and S. Satpathy, Phys. Rev. Lett. **94**, 176805 (2005).
[5] D. R. Hamann, D. A. Muller, and H. Y. Hwang, Phys. Rev. B **73**, 195403 (2006).
[6] S. Okamoto, A. J. Millis, and N. A. Spaldin, Phys. Rev. Lett. **97**, 056802 (2006).
[7] R. Pentcheva and W. E. Pickett, Phys. Rev. Lett. **99**, 016802 (2007).
[8] S. S. A. Seo, W. S. Choi, H. N. Lee, L. Yu, K. W. Kim, C. Bernhard, and T. W. Noh, Phys. Rev. Lett. **99**, 266801 (2007).
[9] H. Ishida and A. Liebsch, Phys. Rev. B **77**, 115350 (2008).
[10] J. B. Goodenough and J.-S. Zhou, Struct. Bonding (Berlin) **98**, 17 (2001).
[11] T. Arima, Y. Tokura, and J. B. Torrance, Phys. Rev. B **48**, 17006 (1993).
[12] Y. Okada, T. Arima, Y. Tokura, C. Murayama, and N. Mori, Phys. Rev. B **48**, 9677 (1993).
[13] Y. Tokura, Y. Taguchi, Y. Okada, Y. Fujishima, T. Arima, K. Kumagai, and Y. Iye, Phys. Rev. Lett. **70**, 2126 (1993).
[14] C. C. Hays, J.-S. Zhou, J. T. Markert, and J. B. Goodenough, Phys. Rev. B **60**, 10367 (1999).
[15] Y. Okimoto, T. Katsufuji, Y. Okada, T. Arima, and Y. Tokura, Phys. Rev. B **51**, 9581 (1995).
[16] C. Eylem, Y.-C. Hung, H. L. Ju, J. Y. Kim, D. C. Green, T. Vogt, J. A. Hriljac, B. W. Eichhorn, R. L. Greene, and L. Salamanca-Riba, Chem. Mater. **8**, 418 (1996).
[17] T. Katsufuji, Y. Taguchi, and Y. Tokura, Phys. Rev. B **56**, 10145 (1997).
[18] T. Higuchi, D. Baba, T. Takeuchi, T. Tsukamoto, Y. Taguchi, Y. Tokura, A. Chainani, and S. Shin, Phys. Rev. B **68**, 104420 (2003).
[19] A. Ohtomo, D. A. Muller, J. L. Grazul, and H. Y. Hwang, Appl. Phys. Lett. **80**, 3922 (2002).
[20] K. H. Kim, D. P. Norton, J. D. Budai, M. F. Chisholm, B. C. Sales, D. K. Christen, and C. Cantoni, Phys. Status Solidi A **200**, 346 (2003).
[21] J. Li, F. B. Wang, P. Wang, M. J. Zhang, H. Y. Tian, and D. N. Zheng, Phys. Rev. B **75**, 195109 (2007).
[22] B. Vilquin, T. Kanki, T. Yanagida, H. Tanaka, and T. Kawai, Appl. Surf. Sci. **244**, 494 (2005).
[23] F. Lichtenberg, D. Widmer, J. G. Bednorz, T. Williams, and A. Reller, Z. Phys. B **82**, 211 (1991).
[24] J. W. Seo, J. Fompeyrine, H. Siegwart, and J.-P. Locquet, Phys. Rev. B **63**, 205401 (2001).
[25] T. Tanaka, T. Akahane, E. Bannai, S. Kawai, N. Tsuda, and Y. Ishizawa, J. Phys. C **9**, 1235 (1976).
[26] P. Pasierb, S. Komornicki, and M. Rekas, J. Phys. Chem. Solids **60**, 1835 (1999).